Oxidation of diethyl ether: Extensive characterization of products formed at low temperature using high resolution mass spectrometry

Nesrine Belhadj, Roland Benoit, Maxence Lailliau, Valentin Glasziou, Philippe Dagaut

Oxidation of diethyl ether: extensive characterization of products formed at low temperature using high resolution mass spectrometry

Nesrine Belhadj[1,2], Roland Benoit[1], Maxence Lailliau[1,2], Valentin Glasziou[1], Philippe Dagaut[1,*]

[1] *CNRS–INSIS, ICARE, 1C avenue de la Recherche Scientifique, 45071 Orléans cedex 2, France*

[2] *Université d'Orléans, Avenue du Parc Floral, 45067 Orléans Cedex 2, France*

*Corresponding author:

Philippe Dagaut Tel : +33 (0)2 38 25 54 66 - email : dagaut@cnrs-orleans.fr

ABSTRACT

The oxidation of a stoichiometric diethyl ether-oxygen-nitrogen mixture containing 5000 ppm of fuel was studied in a jet-stirred reactor at 10 atm and a residence times of 1 s. Experimental temperatures varied stepwise for 440 to 740 K and products were quantified by gas chromatography with TCD and FID, gas chromatography-mass spectrometry, and FTIR. Other experiments in the temperature range 480 to 570 K were performed for characterizing elusive cool flame products. To this end, gas samples were trapped in acetonitrile for flow injection analyses and liquid chromatography-mass spectrometry (Orbitrap Q-Exactive®). For ionization, we used positive and negative atmospheric pressure chemical ionization (APCI). Among fuel-specific products, hydroperoxides and diols ($C_4H_{10}O_3$), carbonyl hydroperoxides ($C_4H_8O_4$), acetic acid, di-keto ethers ($C_4H_6O_3$), cyclic ethers ($C_4H_8O_2$) and highly oxygenated molecules, i.e., keto-dihydroperoxides ($C_4H_8O_6$), keto-trihydroperoxides ($C_4H_8O_8$), di-keto-hydroperoxides ($C_4H_6O_5$), and diketo-dihydroperoxides ($C_4H_6O_7$), were detected. To confirm the presence of –OH or –OOH groups in oxidation products, H/D exchange with D_2O was used. DNPH derivatization was used to identify carbonyls present in samples, especially those with a molecular weight below 50 amu which cannot be detected directly by the mass spectrometer. Chemical kinetic modeling using a mechanism taken from the literature was performed. Although reasonable agreement between the data and the simulations was observed for several species, some discrepancies between experimental and computed mole fractions were observed.

Keywords: jet-stirred reactor, high resolution mass spectrometry, cool-flame, diethyl ether, carbonyl hydroperoxides, ketohydroperoxides, highly oxygenated molecules.

1. Introduction

Biofuels, obtained from renewable feedstocks, are considered environmentally friendly alternatives to fossil fuels. Consequently, their production has attracted considerable scientific attention. Diethyl ether (DEE) is among these biofuels of interest [1]. Its kinetics of oxidation has already been the topic of several studies [2-6]. The oxidation of diethyl ether in a jet-stirred reactor at elevated pressure and low temperature has been studied previously in this laboratory [4]. However, only stable products were measured whereas elusive oxygenates such as carbonyl hydroperoxides, also called ketohydroperoxides (KHPs), and highly oxygenated molecules (HOMs) could not be observed using benchtop gas chromatography and mass spectrometry. Tran et al. [6] reported the formation of more products, detected by gas chromatography and mass spectrometry, molecular beam-mass spectrometry (MBMS) and electron ionization, and by MBMS-photoionization. Among them, fuel-specific products were reported (acetaldehyde, ethanol, ethyl vinyl ether, 2-methyl-1,3-dioxolane, methyl formate, ethyl formate, acetic acid, and acetic anhydride), but no data were presented for carbonyl hydroperoxides and more oxygenated products. Because of its high sensitivity and high resolution, Orbitrap® mass spectrometer is a very appropriate tool for the characterization and identification of complex organic molecules, especially when they are present at trace amounts within complex matrices. Recently, flow injection analyses and ultrahigh-pressure liquid chromatography both coupled to high-resolution mass spectrometry (HRMS) has been used in our laboratory to attempt identifying different KHPs and HOMs isomers formed by oxidation of di-n-propyl ether, di-n-butyl ether, tetrahydrofuran, n-heptane, and a n-heptane-iso-octane mixture [7-10]. In order to better characterize the low-temperature oxidation of diethyl ether, new experiments were performed in a jet-stirred reactor at 10 bar, over a range of

temperatures. Firstly, gas samples were taken and analyzed online and offline by Fourier transform infrared spectrometry (FTIR) and gas chromatography (GC). Secondly, gas samples from JSR experiments were dissolved in acetonitrile and analyzed using a high-resolution mass spectrometer. Flow injection analyses (FIA) or high-pressure liquid chromatography analyses (HPLC) were performed, and an atmospheric pressure chemical ionization ion source (APCI) was used. In addition, different characterization methods were used, i.e., H/D exchange with D_2O to confirm the presence of –OH or –OOH groups in products and derivatization of carbonyl compounds with 2,4-dinitrophenyl hydrazine (2,4-DNPH), known as Brady's reagent [11, 12]. 2,4-DNPH reacts with carbonyl compounds to form corresponding 2,4-dinitrophenyl hydrazone derivatives. This method is commonly applied to measure carbonyl compounds in biological samples [13-17], in ambient air [18-22], and emission by gasoline and Diesel engines [23, 24].

2. Instrumental

2.1 Chemicals reagents and instruments

Diethyl ether (>99.9%, Sigma-Aldrich), acetonitrile UHPLC grade (Fisher Chemical), ultrapure water (Fisher Chemical), phosphoric acid (85% wt. in H_2O, Sigma-Aldrich), 2,4-dinitrophenylhydrazine (97%, Sigma-Aldrich), formic acid (Merck), D_2O (Sigma-Aldrich), Thermo Scientific Vanquish UHPLC system, chromatographic columns Luna® Omega C18 from Phenomenex (1.6µm, 100 Å, 100 x 2.1 mm), Ascentis® Si from Supelco (5 µm, 100 Å, 250 x 2.1 mm), and PGC Hypercarb from Thermo Scientific (5 µm, 150 x 2.1 mm) were used here.

An Orbitrap Q-Exactive® mass spectrometer (Thermo Scientific) with Ion Max® APCI (Thermo Scientific) was used. The spectrometer has a mass accuracy <0.5 ppm and a mass resolution of 140,000.

For JSR experiments, an HPLC pump (Shimadzu LC10 AD VP) with online degasser (Shimadzu DGU-20 A3) was used to pump the fuel. Mass flow controllers were used to send the fuel to the JSR. Nitrogen (99.95%, Air Liquide) and oxygen (99.995, Air Liquide) were used. Gas chromatography analyses were performed using a set of capillary columns (Carboplot P7, Alumina-KCl, DB624, CPSil 5CB) and detectors (flame ionization, FID, thermal conductivity, TCD, and electron impact ionization mass spectrometry, EI-MS). FTIR analyses were performed online with a Nexus 670 (Thermo Nicolet) equipped with a 10 m cell. More details can be found in previous publications [25-27]. Uncertainties on mole fractions were estimated to be of the order of 15%.

2.2 Oxidation of diethyl ether and storage of samples

The oxidation of diethyl ether ($C_4H_{10}O$) was performed in a fused silica jet-stirred reactor (JSR) [28] at 10 atm, at a residence time of 1 s, with initial fuel concentration of 5000 ppm, and an equivalence ratio of 1. The liquid fuel was atomized by a flow of N_2 and vaporized in a heated chamber. The fuel and O_2 were sent separately to the JSR to avoid oxidation before reaching the 4 injectors (1 mm internal diameter nozzles) which provide stirring. For experiments performed over the temperature range 440 to 740 K, gas chromatography and FTIR were used for gas samples speciation. For experiments performed from 480 to 570 K, analyses were performed using APCI-Orbitrap® with FIA and liquid chromatography. There, we focused on the detection of cool flame oxygenated products.

To measure carbonyl hydroperoxides and other low-temperature oxidation products, the sonic probe samples were bubbled into cooled acetonitrile (0°C, 25 mL for 90 min). The resulting solutions were stored in a freezer at -15°C before FIA- and HPLC-HRMS analyses. Compared to samples collected in gaseous form and analyzed by gas chromatography and FTIR, the bubbling technique allows to obtain a liquid sample, which is necessary for liquid chromatography analyses or FIA.

2.3 H/D exchange using D_2O

The fast OH/OD exchange [7-9, 29] was employed to confirm the presence of hydroxy or hydroperoxy groups in oxygenated products. To this end, 150 µL of D_2O were added to 1 mL of liquid samples (70% evaporated); the reaction time was 20 min.

2.4 Sampling and Preparation of 2,4-dinitro phenylhydrazone derivatives

A fraction of liquid samples was derivatized using 2,4-DNPH. A saturated solution of 2,4-DNPH (0.1 mol. L^{-1}) was prepared by dissolving 2 g in 100 mL of acetonitrile. This solution was stirred and then treated in an ultrasonic bath at room temperature for 30 min. Carbonyls present in samples must be

protonated to react with 2,4-DNPH. Therefore, 20 µL of a diluted solution of phosphoric acid (50 µL of H_3PO_4 in 1 mL of ACN) was used to adjust samples pH between 2.8 and 3. Then 20 µL of a 2,4-DNPH solution was added to the samples. The reaction between 2,4-DNPH and carbonyls is a nucleophilic addition followed by elimination of water and formation of 2,4-dinitrophenyl hydrazone, e.g. for KHPs:

$$C_4H_8O_4 + C_6H_6O_4N_4 \leftrightarrows H_2O + C_{10}H_{12}O_7N_4$$

The reaction mechanism of derivatization is detailed in the Supplementary Material (Figure S1).

2.5 Characterization of carbonyl hydroperoxides and highly oxygenated molecules: FIA-MS and HPLC-MS/MS analyses

Flow injection analyses were carried out (flow of 3-5 µL/min recorded for 1 min for data averaging). Atmospheric pressure chemical ionization in positive and negative modes was used to ionize molecules before their detection by an Orbitrap Q-Exactive®.

In HPLC analyses, 3 to 5 µL of sample were injected and eluted by a mobile phase consisting in a mixture of water and organic solvents (acetonitrile, methanol) in various proportions and different flow rates. The analytical conditions which allowed obtaining the best chromatograms are presented in the Supplementary Material (Table S1). The different ionization settings for flow injection and liquid chromatography analyses are given in Table 1. Uncertainties of >40% are estimated for reported HRMS data.

Table 1. Ion Max® atmospheric chemical ionization settings

Ionization settings	Injection mode	
	FIA	HPLC
sheath gas flow (a.u)	10	55
auxiliary gas flow (a.u)	2	6
sweep gas flow (a.u)	0	0
vaporizer temperature (°C)	110	150
capillary temperature (°C)	280	300
corona discharge current (µA)	2.8	3
discharge voltage (kV)	4.12	4.2

In order to identify the structure of KHPs and HOMs, MS/MS analyses were performed using a higher energy collisional dissociation cell (HCD). A collision energy of 10 eV was used.

3. Kinetic modeling

The JSR experiments were simulated with the PSR module [30] of the CHEMKIN II package [31]. The experimentally measured temperature was used as input. A recent kinetic reaction mechanism proposed by Tran et al. [6], involving 746 species and 3555 reactions, was used. Both high- and low-T oxidation pathways are included in that scheme. Whereas other mechanisms have been published for the oxidation of DEE [3, 4, 32-34], the formation of products of third O_2 addition on fuel's radicals is only present in the mechanism of Tran et al. This motivated our choice to use that mechanism in the present work where we probed products of 3rd O_2 addition of the radicals from the fuel. Reaction paths were computed for interpreting the results. A schematic representation is shown in Fig. 1.

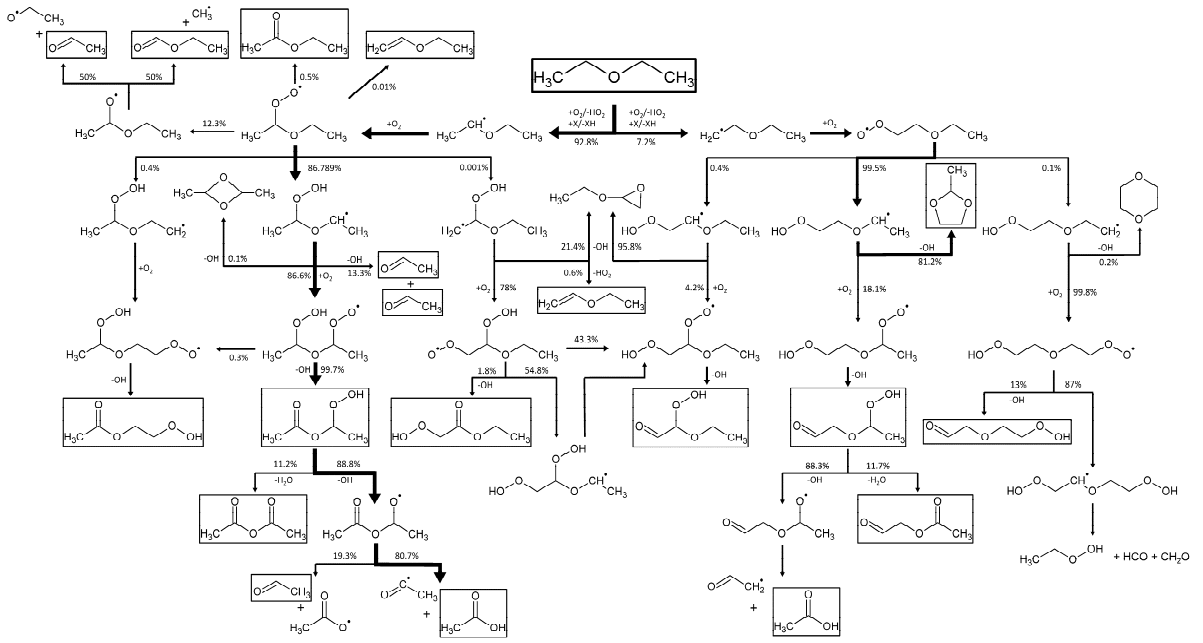

Fig. 1. Reaction paths for the oxidation of DEE at 530 K using the kinetic mechanism of Tran et al. [6]. Species in boxes were detected in the present study. Thick arrows indicate major reaction routes.

One can see from Fig. 1 that the oxidation of diethyl ether mostly proceeds through H-atom abstraction on the CH_2 groups, yielding the α-radical, CH_3-$^{\bullet}$CH-O-CH_2-CH_3, which peroxidizes, yielding CH_3-CH(OO$^{\bullet}$)-O-CH_2-CH_3 which further reacts to yield a range of products such as KHPs, diketones, acetaldehyde, and acetic acid.

4. Results and discussion

JSR experiments with analyses by GC-TCD,-FID,-EI-MS and by FTIR yielded a large set of data which could be compared to simulation results. Mole fraction profiles were measured for the fuel, O_2, H_2, H_2O, CO_2, CO, CH_2O, formic acid, CH_4, C_2H_2, C_2H_4, C_2H_6, acetaldehyde, oxirane, ethanol, acetic acid, acetic anhydride, ketene, propene, ethoxy ethene, ethyl acetate, and 2-methyl-1,3-dioxolane. Figure 2 presents a comparison of experimental data and results of simulations using the mechanism of Tran et al. [6]. One can see that the model represents reasonably well the mole fraction profiles of the fuel, O_2, water, formaldehyde, and carbon dioxide, but tends to underestimate mole fractions of some products, e.g., carbon monoxide, acetic acid, and acetaldehyde. A closer comparison of modeling and experimental results shows that the computed fuel consumption is too fast over the temperature range 480-540 K. This is also true for O_2. One can also note that the computed mole fraction profile for DEE and H_2O cross at 500 K while in the experiments it is observed at ~ 520 K. At 500 K, the consumption of DEE is too fast (Fig. 1). The model indicates that under these conditions DEE is consumed by reaction with OH and methoxy radicals: $CH_3CH_2OCH_2CH_3$ + OH → $CH_3CH_2OCHCH_3$ + H_2O (85%), $CH_3CH_2OCH_2CH_3$ + CH_3O → $CH_3CH_2OCHCH_3$ + CH_3OH (7.7%), and $CH_3CH_2OCH_2CH_3$ + OH → $CH_3CH_2OCH_2CH_2$ + H_2O (7%). OH radicals are produced by peroxy hydroperoxyl radicals decomposition (82%), also forming a KHP, by decomposition of that KHP (12%) and decomposition of an hydroperoxide also yielding 2methyl-1,3-dioxolane (3.8%). OH radicals are mostly consumed via H-atom abstraction on DEE (83%). Methoxy radicals mostly come from the self-reaction of CH_3O_2 which are produced by recombination of methyl radicals and O_2. Methyl radicals, which almost exclusively react by reaction with O_2, are mostly produced by decomposition of CH_3COO (69%) and also by decomposition of ethoxy radicals (16%) and decomposition of $C_2H_5OCH(O)CH_3$ (15%). CH_3COO produce CH_3 and CO_2 by thermal decomposition (100%) whereas they are produced via self-reaction of CH_3CO_3 which results from the peroxidation of CH_3CO. Two reactions yield CH_3CO: OQO → CH_3COOH + CH_3CO (78%) and CH_3CHO + OH → CH_3CO + OH (27%). The too fast oxidation of the fuel must result from an over-production of OH in the mechanism, most likely through the sequence of reactions HOOQ''OOH → OH$^{\bullet}$ + HOOQ'O → OH$^{\bullet}$ + OQ'O which could have been assign too low activation energies.

Finally, the early formation of acetaldehyde (460-520 K) mainly produced via the oxidation pathway of DDE's α-radical (Fig. 1) is not well-captured by the model (dotted line). The model indicates that both ROOH decomposition (CH_3-CH(OOH)-O-$^{\bullet}$CH-CH_3 → 2 CH_3CHO) and [1-(acetyloxy)ethyl]oxidanyl radical decomposition (CH_3-C(=O)-O-CH(O$^{\bullet}$)-CH_3 → $CH_3COO^{\bullet}$ + CH_3CHO) yield acetaldehyde whereas others reactions are less important (% rate of production is given in parenthesis):

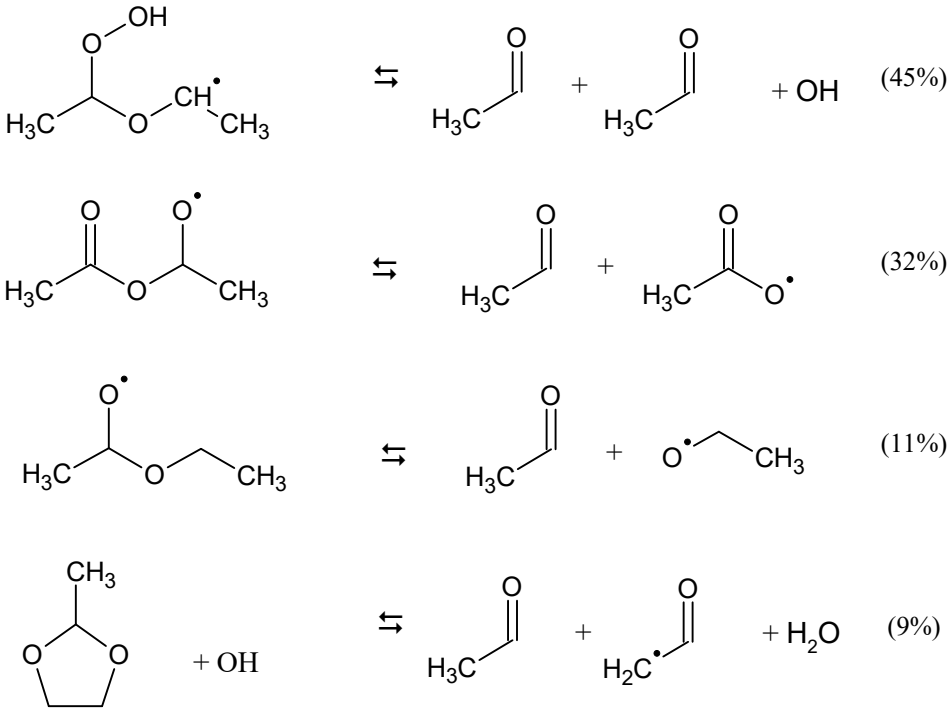

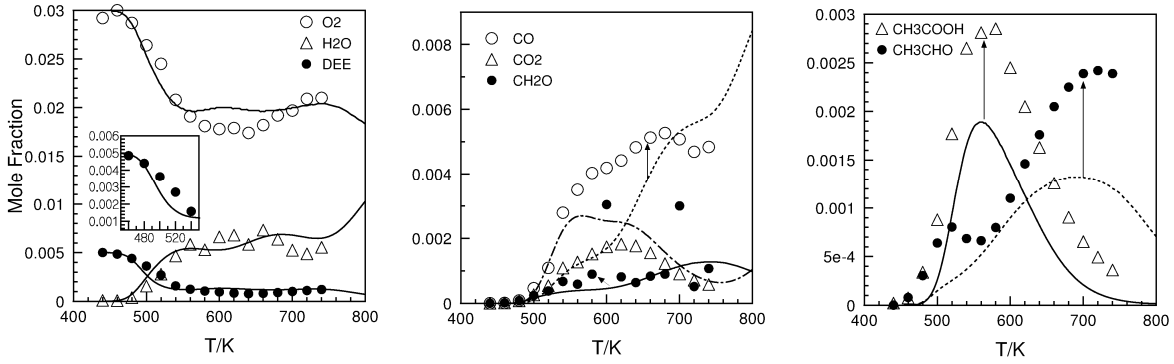

Fig. 2. Oxidation of 5000 ppm of diethyl ether in a JSR at 10 bar. Experimental results (symbols) and computations (lines) are presented.

The analysis of the samples dissolved in acetonitrile allowed plotting the variation of the HRMS signal versus temperature and compare the data with those obtained by gas chromatography. Figure 3 shows an example for the fuel. One can see that the evolution of the fuel concentration versus temperature are in good agreement.

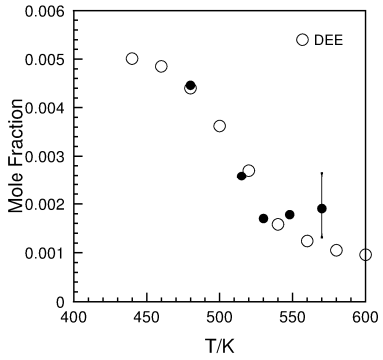

Fig. 3. Consumption of DEE during low-temperature oxidation in a JSR. Open symbols were obtained by GC analyses and black disks by analyses performed in FIA and APCI (+) mode; the HRMS signal was recorded at m/z 75.0802 ($C_4H_{11}O^+$).

In addition to the products detected in the gas-phase by gas chromatography and FTIR, the analysis of liquid samples (gas samples dissolved in acetonitrile) demonstrated the formation of many more oxidation products (Table 2).

Table 2. Compounds detected during the oxidation of 5000 ppm of diethyl ether in a JSR at 530 K and 10 bar. H/D exchange was investigated by adding 150 µL of D_2O to 1 mL of a 70% evaporated liquid sample (reaction time: 20 min). The analyses were carried out in FIA-APCI (+/-) modes. In summary, the following products of diethyl ether oxidation were observed: $C_4H_8O_x$ (1-7), $C_4H_6O_x$ (1-5), $C_4H_4O_x$ (1-3), $C_nH_{2n}O$ (n=3-4), $C_nH_{2n-2}O$ (n=3-4), $C_nH_{2n-4}O$ (n=3-4), $C_nH_{2n+2}O_2$ (n=2,4), $C_nH_{2n}O_2$ (n=2-4), $C_nH_{2n-2}O_2$ (n=2-4), $C_nH_{2n-4}O_2$ (n=3-4), and $C_nH_{2n}O_3$ (n=2-4).

M (g/mole)	Compounds		Ionization mode			
			APCI (+)		APCI (–)	
	Formula	Name	m/z $[M+H]^+$	Signal (a.u)	m/z $[M-H]^-$	Signal (a.u)
56	C_3H_4O	acrolein	57.0334	3.2E5	-	-
58	$C_2H_2O_2$		59.0127	1.7E5	-	-
58	C_3H_6O	acetone	59.0491	7.0E7	57.0345	2.0E5
60	$C_2H_4O_2$	acetic acid and methyl formate	61.0283	9.3E7	59.0138	3.4E8
61	$C_2H_3D_1O_2$	acetic acid-d_1	62.0346	1.0E8	60.0202	1.2E7
68	C_4H_4O		69.0333	2.4E6	-	-
70	$C_3H_2O_2$		71.0126	4.9E4	-	-
70	C_4H_6O		71.0489	3.0E6	69.0345	2.0E5
72	$C_3H_4O_2$		73.0282	6.4E5	71.0138	1.8E6
72	C_4H_8O	Ethoxyethane and isomers	73.0647	3.2E7	71.0502	1.7E5
74	$C_2H_2O_3$		-	-	72.9930	3.1E7
74	$C_3H_6O_2$		75.0439	7.4E6	73.0294	1.6E6
74	$C_4H_{10}O$	DEE	75.0802	4.1E8	-	-
76	$C_2H_4O_3$		77.0230	6.6E6	75.0087	2.9E8
78	$C_2H_6O_3$		79.0387	5.6E6	77.0243	9.3E6
84	$C_4H_4O_2$		85.0281	1.0E6	83.0138	1.9E4
86	$C_4H_6O_2$		87.0438	3.5E7	85.0294	4.6E5

88	$C_3H_4O_3$		89.0230	6.1E6	87.0087	1.0E6
88	$C_4H_8O_2$	ethyl acetate, cyclic ethers isomers, 2-methyl-1,3-dioxalane	89.0594	1.1E7	87.0451	1.4E6
90	$C_3H_6O_3$		91.0387	3.8E5	89.0244	1.5E7
90	$C_2H_2O_4$		-	-	88.9880	9.7E5
92	$C_2H_4O_4$		93.0181	1.1E5	91.0036	6.6E7
94	$C_2H_6O_4$		-	-	93.0192	1.9E7
100	$C_4H_4O_3$		101.0231	6.7E6	99.0087	9.7E5
102	$C_3H_2O_4$		-	-	100.9880	1.3E6
102	$C_4H_6O_3$	diketones (acetic anhydride and isomers)	103.0386	6.3E7	101.0243	4.5E6
104	$C_3H_4O_4$		105.0180	4.2E5	103.0036	1.2E7
104	$C_4H_8O_3$		105.0543	6.2E7	103.0400	3.4E7
105	$C_4H_7D_1O_3$		106.0607	6.7E7	104.0456	8.3E6
106	$C_4H_6D_2O_3$		107.0671	1.9E7	-	-
106	$C_3H_6O_4$		107.0336	7.6E5	105.0192	5.9E6
106	$C_4H_{10}O_3$	diols or ROOH	107.0699	2.3E7	-	-
107	$C_4H_9D_1O_3$	diols or ROOH-d_1	108.0764	5.2E7	-	-
108	$C_4H_8D_2O_3$	diols-d_2	109.0827	2.1E7	-	-
108	$C_3H_8O_4$		-	-	107.0349	8.5E5
108	$C_2H_4O_5$		-	-	106.9985	9.5E5
110	$C_2H_6O_5$		-	-	109.0141	4.0E6
116	$C_4H_4O_4$	triketones and isomers	117.0180	3.7E3	115.0036	2.7E5
118	$C_4H_6O_4$		119.0336	8.0E6	117.0193	1.6E8
120	$C_4H_8O_4$	KHP	121.0492	9.0E6	119.0350	2.4E6
121	$C_4H_7D_1O_4$	KHP-d_1	122.0558	1.7E7	120.0414	2.2E6
122	$C_3H_6O_5$		-	-	121.0142	4.9E6
124	$C_3H_8O_5$		-	-	123.0298	1.6E6
130	$C_4H_2O_5$	tetraketones and isomers	-	-	-	-
134	$C_4H_6O_5$	diketo hydroperoxide	135.0289	1.3E4	133.0142	4.7E5
135	$C_4H_5D_1O_5$	diketo hydroperoxide-d_1	136.0353	1.4E5	134.0207	4.5E6
136	$C_4H_8O_5$		137.0446	1.2E4	135.0299	7.9E6
138	$C_3H_6O_6$		-	-	137.0090	2.9E6
138	$C_4H_{10}O_5$	tetra-ol or di-hydroperoxides	-	-	137.0454	4.4E7
139	$C_4H_9D_1O_5$	tetra-ol or di-hydroperoxides-d_1	-	-	138.0520	8.6E6
140	$C_4H_8D_2O_5$	tetra-ol or di-hydroperoxides-d_2	-	-	139.0582	5.5E5
141	$C_4H_7D_3O_5$	tetra-ol -d_3	-	-	140.0645	5.6E3

142	$C_4H_6D_4O_5$	tetra-ol -d_4	-	-	141.0706	‡
140	$C_3H_8O_6$		-	-	139.0247	3.0E6
148	$C_4H_4O_6$	triketo-hydroperoxide	-	-	-	-
149	$C_4H_3D_1O_6$	triketo-hydroperoxide-d_1	-	-	-	-
152	$C_4H_8O_6$	keto dihydroperoxides	153.0394	1.1E3	151.0247	2.8E6
153	$C_4H_7D_1O_6$	keto dihydroperoxide-d_1	154.0456	‡	152.0312	3.5E6
154	$C_4H_6D_2O_6$	keto dihydroperoxide-d_2	155.0519	‡	153.0375	6.2E6
154	$C_4H_{10}O_6$		-	-	153.0404	6.2E6
166	$C_4H_6O_7$	diketo dihydroperoxide	-	-	165.0041	8.9E2
167	$C_4H_5D_1O_7$	diketo dihydroperoxide-d_1	-	-	166.0105	3.6E4
168	$C_4H_4D_2O_7$	diketo dihydroperoxide-d_2	-	-	167.0166	‡
168	$C_4H_8O_7$		-	-	167.0196	1.5E5
184	$C_4H_8O_8$	keto trihydroperoxides	-	-	183.0149	8.2E2
185	$C_4H_7D_1O_8$	keto trihydroperoxide-d_1	-	-	184.0208	6.3E2
186	$C_4H_6D_2O_8$	keto trihydroperoxide-d_2	-	-	185.0276	1.8E3
187	$C_4H_5D_3O_8$	keto trihydroperoxide-d_3	-	-	186.0338	6.6E3

Note: - not detected; ‡ below detection limit; When no identification of chemicals is given, see Table S2 (Supplementary Material) for tentative identification.

A wide range of molecules such as alkenes deriving from diethyl ether, e.g., ethoxyethene (Fig. 4), carbonyls, such as formaldehyde and acetaldehyde, were observed. Carbonyls having a molecular weight less than 50 amu, could not be detected directly by the Orbitrap-Q-Exactive mass spectrometer. Thus, chemical derivatization of ketones and aldehydes using 2,4-DNPH was used to improve their detection. Table S3 (Supplementary Material) illustrates the results obtained for species having a carbonyl function.

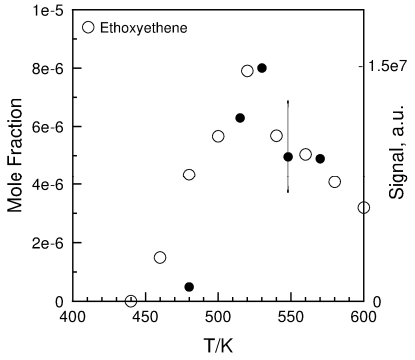

Fig. 4. Formation of ethoxyethene C_4H_8O during the low-T oxidation of DEE in a JSR by GC analyses (open symbols) and HRMS (black disks). The integrated signal of the $C_4H_9O^+$ ion (m/z 73.0647) obtained by FIA/APCI (+) is compared to the gas chromatography measurements.

We also detected diols and hydroperoxides, $C_4H_{10}O_3$ (Table 2, Fig. 5). Jensen et al. [35] proposed that diols are produced by decomposition of di-hydroperoxides [35] while hydroperoxides can result from H-atom abstraction by RO_2, formed by peroxidation of the α and β fuel's radicals (Table 3):

$$R^{\bullet} + O_2 \leftrightarrows RO_2^{\bullet}$$

$$RO_2^{\bullet} + R'H \rightarrow ROOH + R''$$

$$RO_2^{\bullet} + HO_2^{\bullet} \rightarrow ROOH + O_2$$

Figure 5a shows that two H/D exchanges occurred, which indicates the likely presence of diols in the samples. Figure 5b compares the simulated formation of ROOH as a function of temperature and HRMS signal for $C_4H_{10}O_3$. One can see the variation of both HRMS signal and computed $C_4H_{10}O_3$ mole fractions follow the same trend versus temperature.

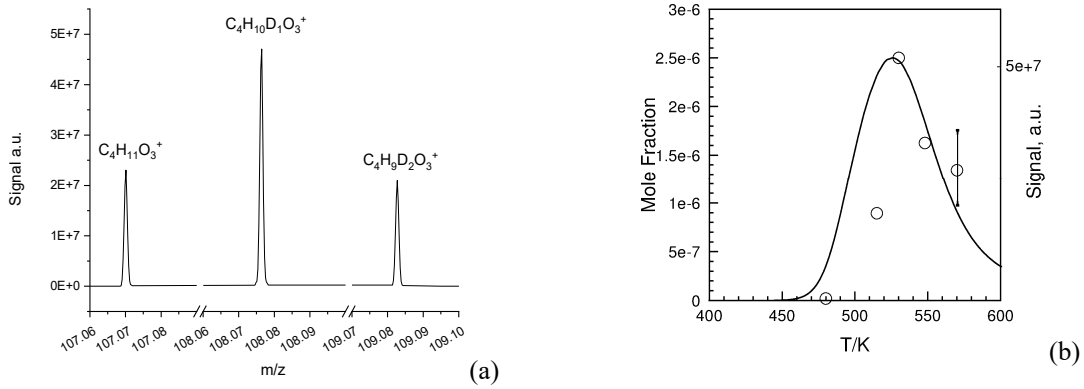

Fig. 5. (a) Mass spectrum showing the formation of $C_4H_{10}DO_3^+$ (m/z 108.0764) and $C_4H_9D_2O_3^+$ (m/z 109.0827) after H/D diols-hydroperoxides exchange with D_2O. Analyses were performed in FIA/APCI (+). No signal for $C_4H_{10}DO_3^+$ and $C_4H_9D_2O_3^+$ could be observed before reaction with D_2O; (b) Formation of $C_4H_{10}O_3$ during the low temperature oxidation of DEE in a JSR (data: circles, simulation: line). The integrated signal was obtained in FIA/APCI positive mode of $C_4H_{11}O_3^+$(m/z 107.0699) ion.

The formation of carbonyl hydroperoxides resulting from second O_2 addition on the fuel's radicals (R) was investigated. Their formation proceeds through the following reactions:

$$RO_2^{\bullet} \leftrightarrows {}^{\bullet}QOOH$$

$${}^{\bullet}QOOH + O_2 \leftrightarrows {}^{\bullet}OOQOOH$$

$${}^{\bullet}OOQOOH \leftrightarrows HOOQ^{\bullet\prime}OOH$$

This last reaction is followed by the decomposition of $HOOQ^{\bullet\prime}OOH$ yielding the hydroxyl radical and a carbonyl hydroperoxide ($C_4H_8O_4$):

$$HOOQ^{\bullet\prime}OOH \rightarrow HOOQ'O + {}^{\bullet}OH.$$

Carbonyl hydroperoxides deriving from the oxidation of diethyl ether were detected in this work (Table 2, Fig. 6). Their chemical structures are given in Table 3. According to the modeling, the most important KHP is by far isomer (a), followed by isomers (c) and (e) formed at similar concentrations. The model predicts negligible formation of the 3 other isomers.

Table 3. Chemical structure of DEE's radicals and carbonyl hydroperoxides produced in oxidation experiments.

Initial radicals formed by H-atom abstraction on DEE	
α position 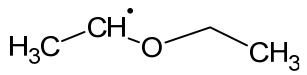	β position 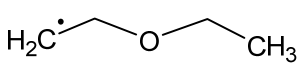
KHPs structure	
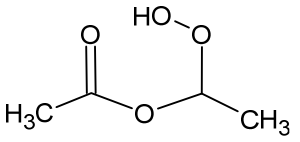 (a)	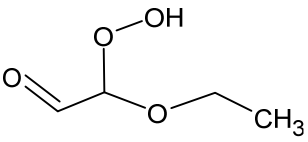 (d)
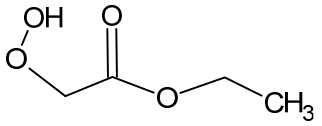 (b)	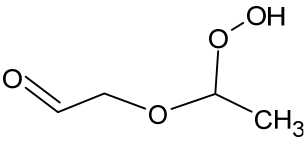 (e)
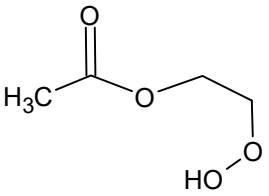 (c)	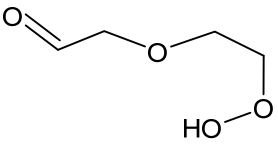 (f)

Figure 6b shows that the model predicts the formation of KHP (line) at too low a temperature compared to the experimental data (circles). This must be due to the aforementioned too fast computed conversion of DEE below 540 K.

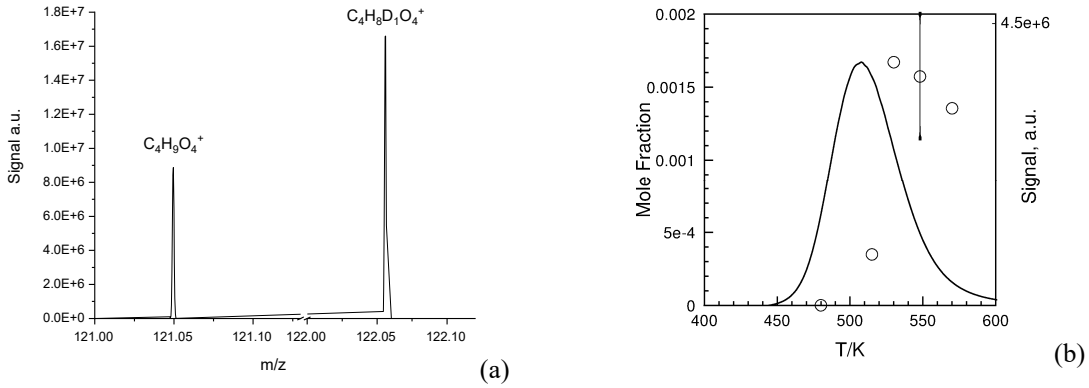

Fig. 6. (a) Mass spectrum showing the formation of $C_4H_8DO_4^+$ (m/z 122.0558) after H/D exchange with D_2O; (b) Formation of $C_4H_9O_4^+$ (m/z 121.0492) ion during the low temperature oxidation of DEE in a JSR (data: circles; simulation: line). Analyses were performed in FIA and APCI (+)

HPLC-MS/MS analyses were performed to separate and identify KHP isomers. Different chromatographic columns were used in HPLC and UHPLC modes. With an UHPLC Luna® C18 column operating in reverse phase mode, we were not able to optimize the separation of KHP isomers, which is probably because of their low molecular weight. Although PGC Hypercarb columns have been frequently used to separate isomers [36-38], we could not achieve the separation of KHPs with that column. However, using an HPLC Silica Ascentis polar column, we could achieve a separation of KHPs

and several oxygenated molecules. Figure 7 presents a chromatogram obtained using an Ascentis® Si column; the analytical conditions are given in Table S1 of the Supplementary Material.

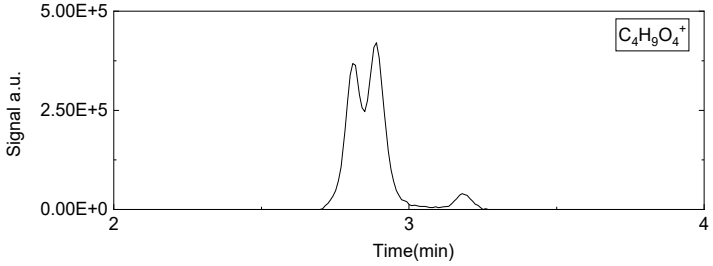

Fig. 7. Formation of KHP during DEE oxidation in a JSR. The chromatogram was recorded at m/z 121.0492 ($C_4H_9O_4^+$) using APCI positive mode. The separation of isomers was obtained with HPLC Ascentis Silica column.

HPLC/MS APCI (+) analyses showed the formation of at least 3 carbonyl hydroperoxides, with possible co-elution of several isomers in peaks at Rt equal to 2.81 and 2.89 min.

MS/MS analyses using an HCD with fragmentation energy of 10 eV generated two fragmentation mass spectra corresponding to the chromatographic peaks at Rt 2.81 and 2.89 min. Some significant fragments could be identified with mass accuracy <0.5 ppm and confirmed the general molecular structure of KHP (Table S4 in Supplementary Material), but we could not identify precisely which isomers were present. This is due to the formation of common fragments from the isomers and to the formation of fragments resulting from molecular rearrangements. In addition, the fragmentation of $C_4H_8O_4$ forms fragments with m/z < 50 which are not detected by our HRMS.

The Korcek mechanism [35, 39] which transforms γ-carbonyl hydroperoxides into stable products (e.g., acetic acid here) can modify fuel ignition [40]. This mechanism is given in Figure 8a. Acetic acid was observed in this work (Table 2). It was detected by FTIR, GC, liquid chromatography, and by comparing the retention times obtained for $C_2H_4O_2$ isomers with that of an acetic acid standard (Fig. S2 in the Supplementary Material).

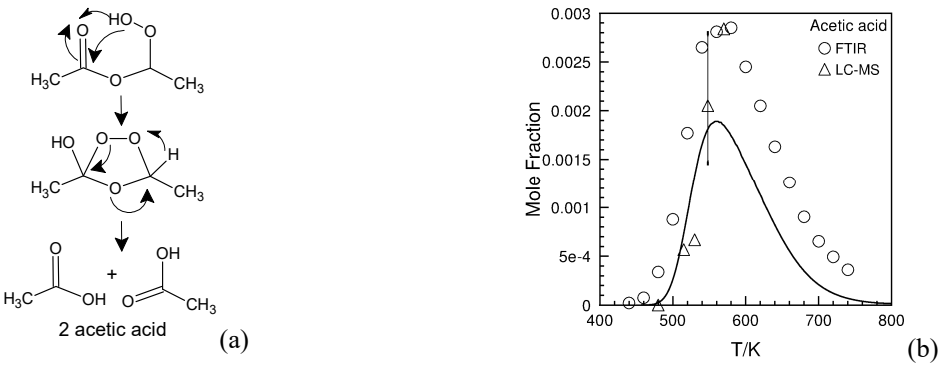

Fig. 8. (a) Formation of acetic acid by decomposition of diethyl ether's γ-carbonyl-hydroperoxides, according to the Korcek mechanism; (b) comparison of modeling results (line) and data (symbols). The HPLC-MS data were scaled to the GC-FID data.

A comparison of computed and experimental results for acetic acid is shown in Fig. 8b. Acetic acid is mainly produced through a sequence of reactions starting from the oxidation of the DEE α-radical (Fig. 1). One can see the model underestimates the peak concentration of acetic acid. The HRMS data are only qualitative; they were scaled to the FTIR data to be presented in Fig. 8b.

Carbonyl hydroperoxides can undergo further chemical transformations yielding diketones [7, 8]. In the present work, diketones ($C_4H_6O_3$) including acetic anhydride, deriving from the oxidation of diethyl ether were detected in both GC and HPLC- or FIA-HRMS (Table 2). Figure 9 presents the variation of the $C_4H_6O_3$ diketones signal at m/z 103.0386 using APCI (+) and recorded as a function of reaction temperature. As can be seen from this figure, diketones reach a maximum concentration near 530 K. The qualitative HRMS data were scaled to the GC data to be presented in this figure.

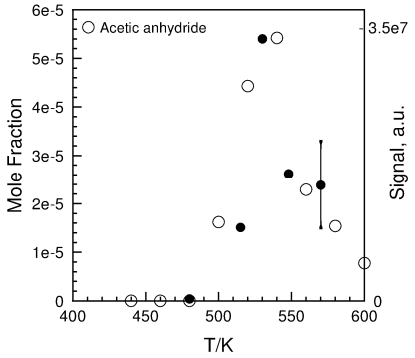

Fig. 9. Formation of diketones $C_4H_7O_3^+$ (m/z 103.0386) ion (black disks) during the low temperature oxidation of DEE in a JSR. Analyses were performed in FIA APCI (+) mode. The HRMS data were compared to the results of gas chromatography analyses of acetic anhydride (circles).

HPLC-MS analyses were performed. They demonstrated the presence of four chromatographic peaks corresponding to four different chemical species (Fig. 10). This result is consistent with the possible formation of 4 diketones during the oxidation of DEE.

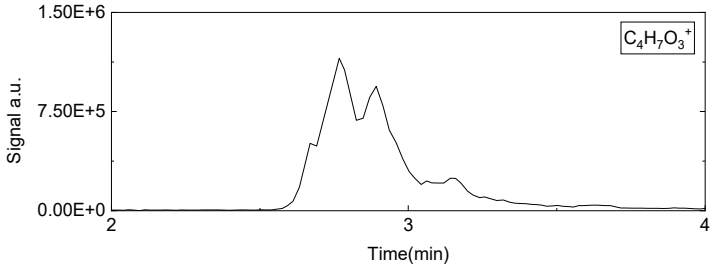

Fig. 10. Formation of diketones $C_4H_6O_3$ during oxidation of DEE in a JSR. The chromatogram was recorded using the MS signal at m/z 103.0386 ($C_4H_7O_3^+$). Chromatographic separation of isomers was obtained using an HPLC Silica column

Cyclic ethers $C_4H_8O_2$, including 2-methyl-1,3-dioxolane, can be formed during DEE oxidation via concerted elimination of OH from alkyl hydroperoxy radicals:

$$^{\bullet}QOOH \rightarrow QO + {}^{\bullet}OH$$

According to the kinetic model, 2-methyl-1,3-dioxolane is formed via OH-elimination and cyclization of HOO-CH_2-O-$^{\bullet}$CH-CH_3. The $C_4H_8O_2$ species also correspond to the chemical formula of a linear molecule, namely ethyl acetate, deriving from the oxidation of the DEE α-radical and decomposition of the corresponding $RO_2^{\bullet}$ (CH_3-CH_2-O-CH(OO$^{\bullet}$)-CH_3). Both 2-methyl-1,3-dioxolane and ethyl acetate were identified in HPLC analyses by injection of standards in acetonitrile (Fig. 12). The presence of ethyl acetate, observed by gas chromatography, was confirmed by chemical derivatization using 2,4-DNPH (Table S3 in the Supplementary Material). Therefore, one could present a comparison of computed mole fractions (lines) and both GC and HPLC-HRMS data for these two products (Fig. 11).

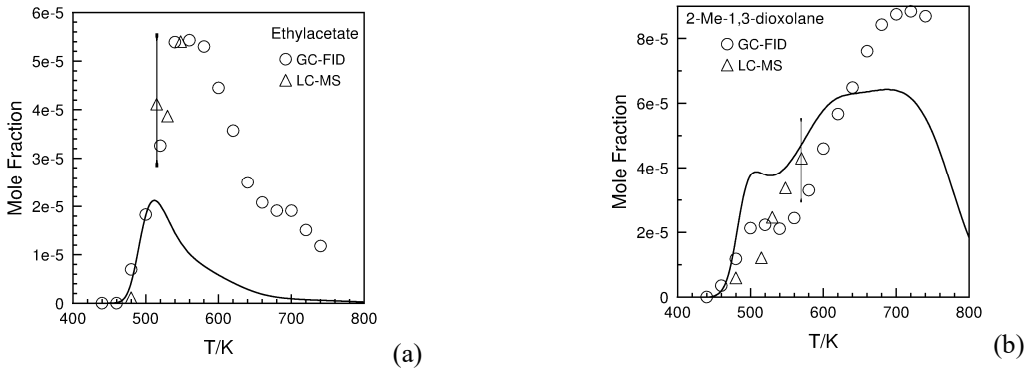

Fig. 11. Formation of ethyl acetate (a) and 2-methyl-1,3-dioxolane (b). These $C_4H_8O_2$ isomers (m/z 89.0594) were observed using HPLC APCI (+) mode. The HPLC-HRMS data were scaled to the GC-FID data.

Figure 11a shows that the kinetic model underpredicts by a factor of ~ 2.5 the maximum mole fraction of ethyl acetate. Also, one can note that scaled HRMS data are in line with those obtained by GC. Figure 11b shows reasonable agreement between computed and measured 2-methyl-1,3-dioxolane mole fractions.

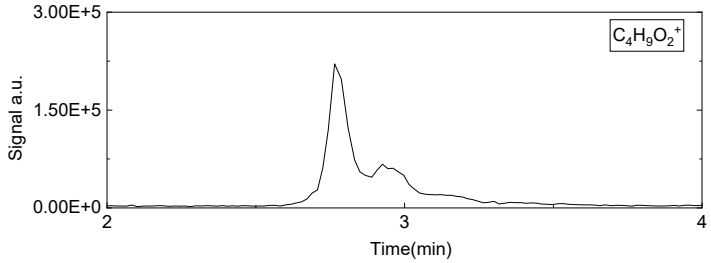

Fig. 12. Chromatogram showing the presence of $C_4H_8O_2$ isomers, including cyclic ethers (Rt of 2-methyl-1,3-dioxolane: 2.90 min), and ethyl acetate (Rt = 2.76 min). The data ($C_4H_9O_2^+$ at m/z 89.0594) were obtained using an HPLC Silica column and APCI (+).

Keto-dihydroperoxy radicals can also react with molecular oxygen (3rd O_2 addition) to yield keto-dihydroperoxides ($C_4H_8O_6$):

$$HOOQ'OOH + O_2 \leftrightarrows (HOO)_2Q'OO^{\bullet}$$

$$(HOO)_2Q'OO^{\bullet} \leftrightarrows (HOO)_2P^{\bullet}OOH$$

$$(HOO)_2P^{\bullet}OOH \rightarrow {}^{\bullet}OH + (HOO)_2P{=}O.$$

Oxidation can proceed further through a 4th O_2 addition to form keto-trihydroperoxides ($C_4H_8O_8$):

$$(HOO)_2P^{\bullet}OOH + O_2 \rightarrow (HOO)_3POO^{\bullet}$$

$$(HOO)_3POO^{\bullet} \leftrightarrows (HOO)_3P^{\bullet\prime}OOH$$

$$(HOO)_3P^{\bullet\prime}OOH \rightarrow {}^{\bullet}OH + (HOO)_3P'{=}O.$$

Among the products detected in this work, highly oxygenated molecules with 5 to 8 oxygen atoms (molecular weight up to 184) were observed: keto-dihydroperoxides ($C_4H_8O_6$), keto-trihydroperoxides ($C_4H_8O_8$), di-keto-hydroperoxides ($C_4H_6O_5$), and di-keto-dihydroperoxides ($C_4H_6O_7$). HOMs formation could have noticeable effect on ignition, as shown in previous computations [41]. H/D exchange with D_2O was used to determine the number of -OOH groups in these highly oxygenated products (Table 2). The results show that these highly oxygenated molecules reach a maximum at a temperature of 530 K (Fig. 13).

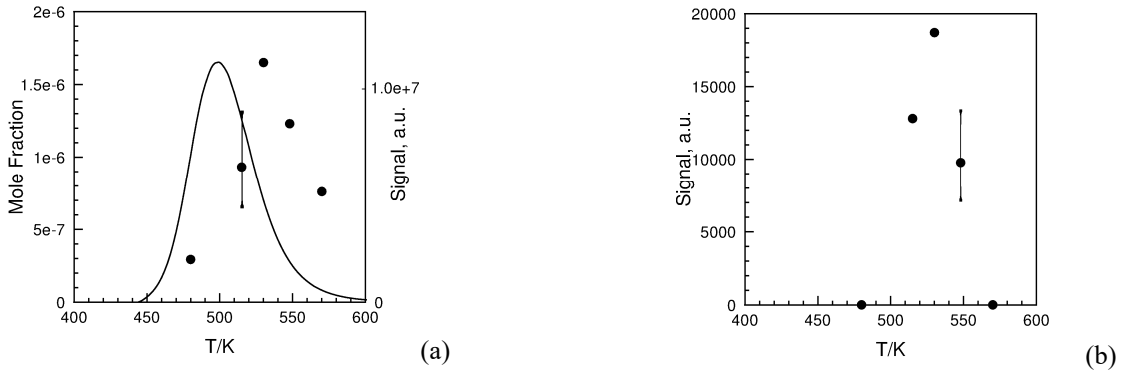

Fig. 13. Formation of highly oxygenated molecules during the low temperature oxidation of DEE in a JSR: (a) keto-dihydroperoxides $C_4H_8O_6$ corresponding to $C_4H_7O_6^-$ ions (m/z 151.0247). The HRMS data are scaled to the maximum computed mole fraction of the sum of HOMs in the model; (b) keto-trihydroperoxides $C_4H_8O_8$ corresponding to $C_4H_7O_8^-$ ions (m/z 183.0149). Analyses were performed in FIA APCI (-).

Figure 13a shows a comparison between simulations (lines) and qualitative HRMS data (symbols). In the model, three HOM isomers were considered (CH_3-CH(OOH)-O-C(=O)-COOH, CH_3-C(=O)-O-CH(OOH)-CH_2-OOH, and O=CH-CH_2-O-CH$(OOH)_2$). As already observed for other products, the

model predicts a peak concentration at ~ 30 K lower than in the experiments. The experimental profiles obtained for $C_4H_7O_6^-$ and $C_4H_7O_8^-$ ions have similar shape, but differ by two orders of magnitude (Fig. 13b). HPLC-MS analysis was performed to demonstrate the presence of several isomers of keto-dihydroperoxides (Fig. 14).

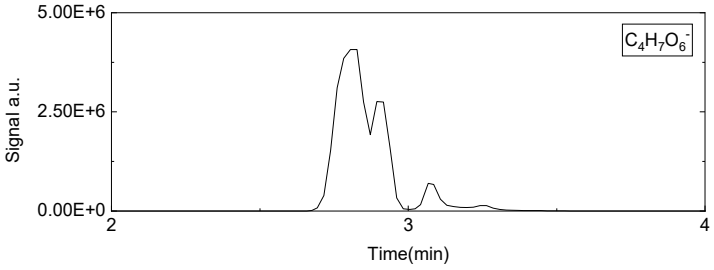

Fig. 14. Chromatogram showing the presence of $C_4H_8O_6$ keto-dihydroperoxides isomers. The data were obtained using an HPLC Silica column and APCI negative mode ($C_4H_7O_6^-$ at m/z 151.0247).

Di-keto-hydroperoxides ($C_4H_6O_5$) and di-keto-dihydroperoxides ($C_4H_6O_7$) result from the decomposition of keto-dihydroperoxides ($C_4H_8O_6$) and keto-trihydroperoxides ($C_4H_8O_8$) respectively. An example of these decomposition reactions is presented in Figure S3 (Supplementary Material). The variation of the HRMS signals recorded as a function of the JSR temperature is shown in Figure 15. The profiles obtained for $C_4H_5O_5^-$ and $C_4H_5O_7^-$ ions are similar but differ by a factor of ca. 200.

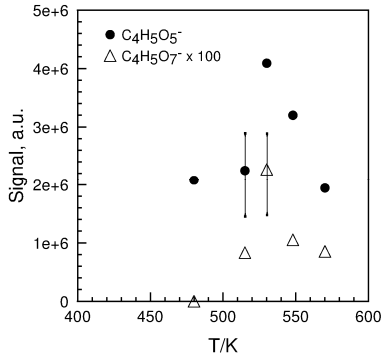

Fig. 15. Formation of highly oxygenated molecules during the low temperature oxidation of DEE in a JSR: (●) di-keto-hydroperoxides $C_4H_6O_5$ corresponding to $C_4H_5O_5^-$ ion (m/z 133.0142). (Δ) di-keto-dihydroperoxides $C_4H_6O_7$ corresponding to $C_4H_5O_7^-$ ion (m/z 165.0041). Analyses were performed in FIA APCI (-).

5. Conclusions and perspectives

The present article reports new experimental results for the oxidation of a stoichiometric diethyl ether-oxygen-nitrogen mixture in a jet-stirred reactor at 10 atm, an equivalence ratio of 1, a residence times of 1 s, and temperatures ranging from 440 to 740 K. For speciation, a set of techniques was use: gas chromatography with TCD, FID, and MS, FTIR, FIA-and HPLC-HRMS and soft ionization (APCI +/-), H/D exchange with D_2O to confirm the presence of –OH or –OOH functions in the products, and DNPH derivatization to identify carbonyl compounds.

DEE, O_2, H_2, H_2O, CO_2, CO, CH_2O, formic acid, CH_4, C_2H_2, C_2H_4, C_2H_6, acetaldehyde, oxirane, ethanol, acetic acid, acetic anhydride, ketene, propene, ethoxy ethene, ethyl acetate, and 2-methyl-1,3-dioxolane were detected in the gas phase and quantified. Moreover, hydroperoxides and diols ($C_4H_{10}O_3$), keto-hydroperoxides ($C_4H_8O_4$), acetic acid, di-keto ethers ($C_4H_6O_3$), cyclic ethers ($C_4H_8O_2$) and highly oxygenated molecules: keto-dihydroperoxides ($C_4H_8O_6$), keto-trihydroperoxides ($C_4H_8O_8$), di-keto-hydroperoxides ($C_4H_6O_5$), and diketo-dihydroperoxides ($C_4H_6O_7$) were detected after dissolution of gas samples in acetonitrile and HRMS analyses. Whereas one could expect these species to be formed, based on our previous measurements concerning the oxidation of di-n-propyl and di-n-butyl ethers, we also observed products with a number of carbon atoms larger or even much larger than expected under the present experimental conditions: $C_nH_{2n}O$ (n=3-5), $C_nH_{2n-2}O$ (n=3-9), $C_nH_{2n-4}O$ (n=3-12), $C_nH_{2n}O_2$ (n=2-6), $C_nH_{2n-2}O_2$ (n=2-16), $C_nH_{2n-4}O_2$ (n=3-14), and $C_nH_{2n}O_3$ (n=2-10). This result seems to indicate

similitude with smog chamber experimental results, i.e., formation of oligomers [42]. Research is underway to consolidate these observations.

Kinetic simulations were performed with detailed kinetic reaction mechanism taken from the literature. Some discrepancies between experimental and modeling results were observed. Most of them were ascribed to an overestimation of DEE rate of oxidation below 560 K. The present results should be useful for kinetic mechanism improvements.

Acknowledgements

The authors gratefully acknowledge funding from the Labex Caprysses (convention ANR-11-LABX-0006-01) and from the Region Centre Val de Loire, EFRD, and CPER (projects PROMESTOCK and APROPOR-E). We thank Prof. P. Favetta, University of Orléans, for lending us a chromatographic column.

References

[1] B. Bailey; J. Eberhardt; S. Goguen; J. Erwin, Diethyl Ether (DEE) as a Renewable Diesel Fuel. SAE Technical Paper 972978, (1997)

[2] D. J. Waddington; A. C. Egerton, The gaseous oxidation of diethyl ether, Proceedings of the Royal Society of London. Series A. Mathematical and Physical Sciences 252 (1269) (1959) 260-272.

[3] K. Yasunaga; F. Gillespie; J. M. Simmie; H. J. Curran; Y. Kuraguchi; H. Hoshikawa; M. Yamane; Y. Hidaka, A Multiple Shock Tube and Chemical Kinetic Modeling Study of Diethyl Ether Pyrolysis and Oxidation, J. Phys. Chem. A 114 (34) (2010) 9098-9109.

[4] Z. Serinyel; M. Lailliau; S. Thion; G. Dayma; P. Dagaut, An experimental chemical kinetic study of the oxidation of diethyl ether in a jet-stirred reactor and comprehensive modeling, Combust. Flame 193 (2018) 453-462.

[5] L. S. Tran; Y. Y. Li; M. R. Zeng; J. Pieper; F. Qi; F. Battin-Leclerc; K. Kohse-Hoinghaus; O. Herbinet, Elevated pressure low-temperature oxidation of linear five-heavy-atom fuels: diethyl ether, n-pentane, and their mixture, Zeitschrift Fur Physikalische Chemie-International Journal of Research in Physical Chemistry & Chemical Physics 234 (7-9) (2020) 1269-1293.

[6] L.-S. Tran; O. Herbinet; Y. Li; J. Wullenkord; M. Zeng; E. Bräuer; F. Qi; K. Kohse-Höinghaus; F. Battin-Leclerc, Low-temperature gas-phase oxidation of diethyl ether: Fuel reactivity and fuel-specific products, Proc. Combust. Inst. 37 (1) (2019) 511-519.

[7] N. Belhadj; R. Benoit; P. Dagaut; M. Lailliau; Z. Serinyel; G. Dayma; F. Khaled; B. Moreau; F. Foucher, Oxidation of di-n-butyl ether: Experimental characterization of low-temperature products in JSR and RCM, Combust. Flame 222 (2020) 133-144.

[8] N. Belhadj; R. Benoit; P. Dagaut; M. Lailliau, Experimental characterization of n-heptane low-temperature oxidation products including keto-hydroperoxides and highly oxygenated organic molecules (HOMs), Combust. Flame (2021) https://doi.org/10.1016/j.combustflame.2020.10.021.

[9] N. Belhadj; R. Benoit; P. Dagaut; M. Lailliau; Z. Serinyel; G. Dayma, Oxidation of di-n-propyl ether: Characterization of low-temperature products, Proc. Combust. Inst. 38 (2021) https://doi.org/10.1016/j.proci.2020.06.350.

[10] N. Belhadj; R. Benoit; P. Dagaut; M. Lailliau, Experimental Characterization of Tetrahydrofuran Low-Temperature Oxidation Products Including Ketohydroperoxides and Highly Oxygenated Molecules, Energy Fuels 10.1021/acs.energyfuels.0c03291 (2021)

[11] O. L. Brady; G. V. Elsmie, The use of 2:4-dinitrophenylhydrazine as a reagent for aldehydes and ketones, Analyst 51 (599) (1926) 77-78.

[12] O. L. Brady, CIII.—The use of 2 : 4-dinitrophenylhydrazine as a reagent for carbonyl compounds, Journal of the Chemical Society (Resumed) (0) (1931) 756-759.

[13] R. P. Dator; M. J. Solivio; P. W. Villalta; S. Balbo, Bioanalytical and Mass Spectrometric Methods for Aldehyde Profiling in Biological Fluids, Toxics 7 (2) (2019) 32.

[14] D. Weber; M. J. Davies; T. Grune, Determination of protein carbonyls in plasma, cell extracts, tissue homogenates, isolated proteins: Focus on sample preparation and derivatization conditions, Redox Biology 5 (2015) 367-380.

[15] J.-F. Liu; B.-F. Yuan; Y.-Q. Feng, Determination of hexanal and heptanal in human urine using magnetic solid phase extraction coupled with in-situ derivatization by high performance liquid chromatography, Talanta 136 (2015) 54-59.

[16] C. D. Georgiou; D. Zisimopoulos; V. Argyropoulou; E. Kalaitzopoulou; G. Salachas; T. Grune, Protein and cell wall polysaccharide carbonyl determination by a neutral pH 2,4-dinitrophenylhydrazine-based photometric assay, Redox Biology 17 (2018) 128-142.

[17] B. Yilmaz; A. Asci; K. Kucukoglu; M. Albayrak, Simple high-performance liquid chromatography method for formaldehyde determination in human tissue through derivatization with 2,4-dinitrophenylhydrazine, J. Sep. Sci. 39 (15) (2016) 2963-2969.

[18] S. Kölliker; M. Oehme; C. Dye, Structure Elucidation of 2,4-Dinitrophenylhydrazone Derivatives of Carbonyl Compounds in Ambient Air by HPLC/MS and Multiple MS/MS Using Atmospheric Chemical Ionization in the Negative Ion Mode, Anal. Chem. 70 (9) (1998) 1979-1985.

[19] W. Rosenberger; B. Beckmann; R. Wrbitzky, Airborne aldehydes in cabin-air of commercial aircraft: Measurement by HPLC with UV absorbance detection of 2,4-dinitrophenylhydrazones, Journal of Chromatography B 1019 (2016) 117-127.

[20] C. Zwiener; T. Glauner; F. Frimmel, Method optimization for the determination of carbonyl compounds in disinfected water by DNPH derivatization and LC–ESI–MS–MS, Anal. Bioanal. Chem. 372 (5) (2002) 615-621.
[21] J. Williams; H. Li; A. B. Ross; S. P. Hargreaves, Quantification of the influence of NO2, NO and CO gases on the determination of formaldehyde and acetaldehyde using the DNPH method as applied to polluted environments, Atmos. Environ. 218 (2019) 117019.
[22] S. Takeda; S.-i. Wakida; M. Yamane; K. Higashi, Analysis of lower aliphatic aldehydes in water by micellar electrokinetic chromatography with derivatization to 2,4-dinitrophenylhydrazones, Electrophoresis 15 (1) (1994) 1332-1334.
[23] Z. Yao; X. Jiang; X. Shen; Y. Ye; X. Cao; Y. Zhang; K. He, On-Road Emission Characteristics of Carbonyl Compounds for Heavy-Duty Diesel Trucks, Aerosol and Air Quality Research 15 (3) (2015) 915-925.
[24] R. Li; Z. Wang; G. Xu, Study on Carbonyl Emissions of Diesel Engine Fueled with Biodiesel, International Journal of Chemical Engineering 2017 (2017) 1409495.
[25] P. Dagaut; M. Cathonnet; J. C. Boettner; F. Gaillard, Kinetic Modeling of Propane Oxidation, Combust. Sci. Technol. 56 (1-3) (1987) 23-63.
[26] P. Dagaut; M. Cathonnet; J. C. Boettner; F. Gaillard, Kinetic modeling of ethylene oxidation, Combust. Flame 71 (3) (1988) 295-312.
[27] P. Dagaut; C. Togbe, Experimental and modeling study of the kinetics of oxidation of ethanol-n-heptane mixtures in a jet-stirred reactor, Fuel 89 (2) (2010) 280-286.
[28] P. Dagaut; M. Cathonnet; J. P. Rouan; R. Foulatier; A. Quilgars; J. C. Boettner; F. Gaillard; H. James, A Jet-Stirred Reactor for Kinetic-Studies of Homogeneous Gas-Phase Reactions at Pressures up to 10-Atmospheres (~ 1 MPa), Journal of Physics E-Scientific Instruments 19 (3) (1986) 207-209.
[29] Z. Wang; D. M. Popolan-Vaida; B. Chen; K. Moshammer; S. Y. Mohamed; H. Wang; S. Sioud; M. A. Raji; K. Kohse-Höinghaus; N. Hansen; P. Dagaut; S. R. Leone; S. M. Sarathy, Unraveling the structure and chemical mechanisms of highly oxygenated intermediates in oxidation of organic compounds, Proceedings of the National Academy of Sciences 114 (50) (2017) 13102-13107.
[30] P. Glarborg; R. J. Kee; J. F. Grcar; J. A. Miller in: *PSR: A FORTRAN program for modeling well-stirred reactors.*, SAND86-8209, Sandia National Laboratories, Livermore, CA, 1986
[31] R. J. Kee; F. M. Rupley; J. A. Miller in: *CHEMKIN-II: A Fortran Chemical Kinetics Package for the Analysis of Gas-Phase Chemical Kinetics.*, SAND89-8009, Sandia National Laboratories, Livermore, CA, 1989
[32] E. Hu; Y. Chen; Z. Zhang; J.-Y. Chen; Z. Huang, Ab initio calculation and kinetic modeling study of diethyl ether ignition with application toward a skeletal mechanism for CI engine modeling, Fuel 209 (2017) 509-520.
[33] Z. Tang; L. Zhang; X. Chen; G. Tang, Improved Kinetic Mechanism for Diethyl Ether Oxidation with a Reduced Model, Energy Fuels 31 (3) (2017) 2803-2813.
[34] J. Eble; J. Kiecherer; M. Olzmann, Low-Temperature Autoignition of Diethyl Ether/O2 Mixtures: Mechanistic Considerations and Kinetic Modeling, Zeitschrift für Physikalische Chemie 231 (10) (2017) 1603-1623.
[35] R. K. Jensen; S. Korcek; L. R. Mahoney; M. Zinbo, Liquid-phase autoxidation of organic-compounds at elevated-temperatures .1. stirred flow reactor technique and analysis of primary products from normal-hexadecane autoxidation at 120-degrees-C 180-degrees-C, J. Am. Chem. Soc. 101 (25) (1979) 7574-7584.
[36] P. J. Houghton; T. Z. Woldemariam, Use of a porous graphitic carbon column to separate isomers of piperidino-type chromone alkaloids, Phytochem. Anal. 6 (2) (1995) 85-88.
[37] S. Bieri; E. Varesio; O. Muñoz; J.-L. Veuthey; P. Christen, Use of porous graphitic carbon column for the separation of natural isomeric tropane alkaloids by capillary LC and mass spectrometry, J. Pharm. Biomed. Anal. 40 (3) (2006) 545-551.
[38] J. L. Gundersen, Separation of isomers of nonylphenol and select nonylphenol polyethoxylates by high-performance liquid chromatography on a graphitic carbon column, Journal of Chromatography A 914 (1) (2001) 161-166.
[39] A. Jalan; I. M. Alecu; R. Meana-Paneda; J. Aguilera-Iparraguirre; K. R. Yang; S. S. Merchant; D. G. Truhlar; W. H. Green, New Pathways for Formation of Acids and Carbonyl Products in Low-Temperature Oxidation: The Korcek Decomposition of gamma-Ketohydroperoxides, J. Am. Chem. Soc. 135 (30) (2013) 11100-11114.
[40] E. Ranzi; C. Cavallotti; A. Cuoci; A. Frassoldati; M. Pelucchi; T. Faravelli, New reaction classes in the kinetic modeling of low temperature oxidation of n-alkanes, Combust. Flame 162 (5) (2015) 1679-1691.
[41] Z. D. Wang; S. M. Sarathy, Third O-2 addition reactions promote the low-temperature auto-ignition of n-alkanes, Combust. Flame 165 (2016) 364-372.
[42] A. P. Bateman; S. A. Nizkorodov; J. Laskin; A. Laskin, Time-resolved molecular characterization of limonene/ozone aerosol using high-resolution electrospray ionization mass spectrometry, Phys. Chem. Chem. Phys. 11 (36) (2009) 7931-7942.